

Functional genomics identifies therapeutic targets for MYC-driven cancer

Masafumi Toyoshima^{a,1}, Heather L. Howie^a, Maki Imakura^b, Ryan M. Walsh^{b,2}, James E. Annis^{b,c}, Aaron N. Chang^{b,3}, Jason Frazier^{b,4}, B. Nelson Chau^{b,5}, Andrey Loboda^d, Peter S. Linsley^{b,6}, Michele A. Cleary^{b,7}, Julie R. Park^e, and Carla Grandori^{a,b,c,8}

^aDepartment of Human Biology, Fred Hutchinson Cancer Research Center, Seattle, WA 98109; ^bRosetta Inpharmatics, LLC, Merck & Co., Inc., Seattle, WA 98109; ^cQuellos High Throughput Screening Core, Department of Pharmacology, Institute for Stem Cells and Regenerative Medicine and ^dSeattle Children's Hospital and Department of Pediatrics, University of Washington, Seattle, WA 98109; and ^eMerck & Co., West Point, PA 19486

Edited* by William G. Kaelin, Jr., Harvard Medical School, Boston, MA, and approved April 19, 2012 (received for review December 23, 2011)

MYC oncogene family members are broadly implicated in human cancers, yet are considered “undruggable” as they encode transcription factors. MYC also carries out essential functions in proliferative tissues, suggesting that its inhibition could cause severe side effects. We elected to identify synthetic lethal interactions with c-MYC overexpression (MYC-SL) in a collection of ~3,300 druggable genes, using high-throughput siRNA screening. Of 49 genes selected for follow-up, 48 were confirmed by independent retesting and approximately one-third selectively induced accumulation of DNA damage, consistent with enrichment in DNA-repair genes by functional annotation. In addition, genes involved in histone acetylation and transcriptional elongation, such as *TRRAP* and *BRD4*, were identified, indicating that the screen revealed known MYC-associated pathways. For in vivo validation we selected *CSNK1e*, a kinase whose expression correlated with *MYCN* amplification in neuroblastoma (an established MYC-driven cancer). Using RNAi and available small-molecule inhibitors, we confirmed that inhibition of *CSNK1e* halted growth of *MYCN*-amplified neuroblastoma xenografts. *CSNK1e* had previously been implicated in the regulation of developmental pathways and circadian rhythms, whereas our data provide a previously unknown link with oncogenic MYC. Furthermore, expression of *CSNK1e* correlated with c-MYC and its transcriptional signature in other human cancers, indicating potential broad therapeutic implications of targeting *CSNK1e* function. In summary, through a functional genomics approach, pathways essential in the context of oncogenic MYC but not to normal cells were identified, thus revealing a rich therapeutic space linked to a previously “undruggable” oncogene.

WNT | SHH | PER | PES1 | CECR2

The *MYC* oncogene is a central driver in many human cancers, and its amplification is associated with poor prognosis in breast (1), prostate (2), colon (3), and pediatric cancers such as neuroblastoma (for review see ref. 4). In addition, c-MYC overexpression together with gene amplification has been reported in over 50% of ovarian cancers (5), in ~30% of hepatocellular carcinoma (6), and in a high percentage of small-cell and non-small-cell lung cancer (7). This high frequency of *MYC* family deregulation in human cancers suggests that a strategy to target *MYC*-driven cancers may be relevant for a broad population of patients. Recently, systemic inhibition of MYC using a transgenic mouse model has demonstrated the efficacy of a dominant negative MYC in mediating tumor regression (8). However, *MYC* family members encode a basic helix loop helix type of transcription factors without obvious druggable domains (9), rendering the identification of small-molecule inhibitors a challenge (10). In addition, as MYC oncoproteins carry out essential functions in proliferative tissues (11), prolonged inhibition of MYC function could cause severe toxicity.

Previous studies using a candidate approach have indicated that the fitness of MYC-overexpressing cells (12) and cancers (13–15) is highly dependent upon other genes and pathways, which may not be essential in the context of normal cells, or of cancers driven by different oncogenic signals. These studies also demonstrated that inhibition of these MYC “synthetic lethal” interactions is an effective therapeutic strategy (13). To broadly

identify genes that exhibit a synthetic lethal relation with oncogenic expression of MYC we have used a high-throughput functional genomic approach (16) focused on the druggable genome. As the genetic noise inherent in established cancer cell lines could constitute a potential source of bias, we chose to screen an isogenic pair of primary cells (human foreskin fibroblasts, HFFs), where the only perturbation was overexpression of c-MYC through a retroviral vector (17) and to validate the “hits” in cancer cell contexts. HFFs are unique in that they do not senesce in response to MYC overexpression (17) or introduction of an activated RAS oncogene (18), a property that has been attributed to lack of culture stress. Furthermore, c-MYC overexpression in HFFs recapitulates both the gene expression signatures and cellular phenotypes of MYC-driven cancers (17, 19, 20).

Results

siRNA Screening Identifies a Network of Genes Required for Survival of c-MYC Overexpressing Cells. We used a high-throughput automated approach for testing of an arrayed siRNA library to quantify the effects of siRNAs against a custom-designed collection of ~3,300 druggable genes (9) and 200 microRNAs. We compared the viability of HFF cells stably transduced with a retroviral vector expressing c-MYC (HFF-MYC) and HFF cells with a control empty vector, pBabe (HFF-pBabe) (17) (Fig. 1A shows a schematic of the experimental set-up). The siRNA library collection was designed to target all known human kinases, ubiquitin ligases, DNA repair proteins, and a custom collection of genes involved in cancer pathways, with each target gene being interrogated by a pool of three unique siRNAs. As has been shown in other biological systems, three technical replicates and a one-gene-per-well approach enabled derivation of hits with statistical significance for each gene tested (21, 22). Cell viability was assessed using Alamar Blue staining and was quantified using an EnVision plate reader (Perkin-Elmer). The results of the screen revealed 148 hits, defined according to a Z score of ≥ 2 (23), including 140 genes and eight microRNAs (Fig. 1B). Here, we focus on the 140 gene hits,

Author contributions: M.T., P.S.L., M.A.C., J.R.P., and C.G. designed research; M.T., H.L.H., M.I., R.M.W., J.E.A., and C.G. performed research; B.N.C. and J.F. contributed new reagents/analytic tools; M.T., H.L.H., M.I., R.M.W., J.E.A., A.N.C., A.L., and C.G. analyzed data; and M.T., H.L.H., and C.G. wrote the paper.

The authors declare no conflict of interest.

*This Direct Submission article had a prearranged editor.

Freely available online through the PNAS open access option.

¹Present address: Tohoku University School of Medicine, Dept. of Obstetrics and Gynecology, Sendai, Japan 980-0824.

²Present address: Massachusetts General Hospital Center for Regenerative Medicine and Cancer Center, Boston, MA 02114.

³Present Address: Baylor Institute for Immunology, Dallas, TX 75204.

⁴Present address: Presage Biosciences, Seattle, WA 98109.

⁵Present address: Regulus Therapeutics, Carlsbad, CA 92008.

⁶Present address: AVI BioPharma, Bothell, WA 98021.

⁷Present address: Merck & Co., West Point, PA 19486.

⁸To whom correspondence should be addressed. E-mail: cgrandor@fhcr.org.

This article contains supporting information online at www.pnas.org/lookup/suppl/doi:10.1073/pnas.1121119109/-DCSupplemental.

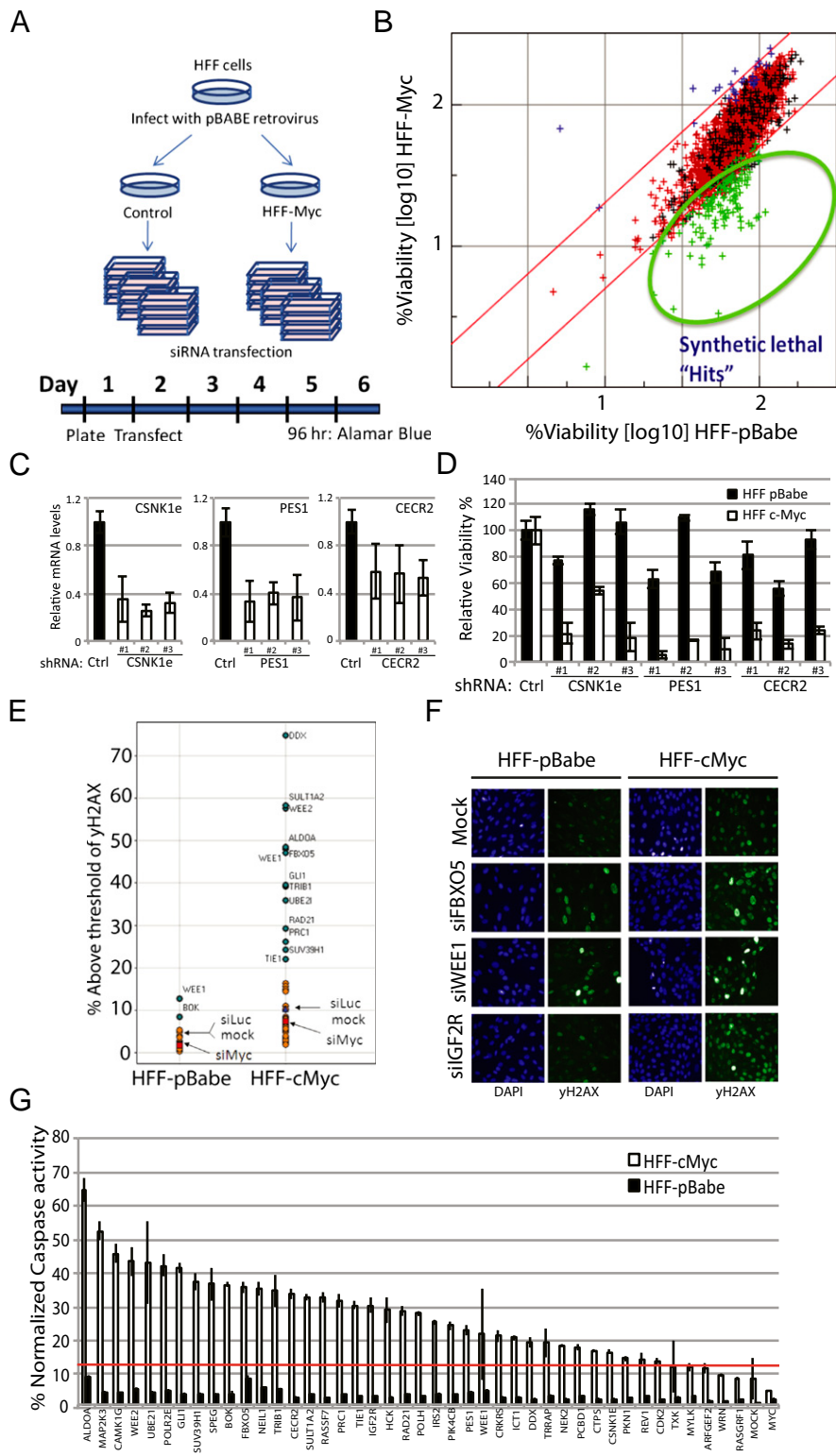


Fig. 1. Identification of synthetic lethal genes with c-MYC overexpression by high-throughput siRNA screening. (A) Graphical schematic of the siRNA screen. Isogenic HFFs were plated, transfected with siRNAs targeting a total of 3,311 genes (1 gene per well), and assessed for viability using an Alamar Blue assay. (B) Graph of normalized viability of HFF-pB and HFF-c-MYC transfected with each siRNA pool (average of three replicates). MYC-SL "hits" (Z score ≥ 2) are highlighted in green. (C) mRNA levels following lentiviral-mediated shRNA knockdown in HFFs of three selected MYC-SL genes, *CSNK1e*, *PES1*, and *CECR2*. (D) Selective loss of viability of HFF-pBabe and HFF-MYC caused by knockdown of the genes shown in C. (E) Quantification of γ -H2AX staining following transduction of HFF-pBabe and HFF-MYC with siRNA pools corresponding to 40 MYC-SL genes. *DDX18*, a known MYC-target gene, and MYC were used as controls. y axis indicates the percent of cells stained with anti- γ -H2AX that scored for nuclear fluorescence levels above a threshold established from negative controls. (F) Representative images of γ -H2AX staining as described in E obtained with an INCell automated microscope (10 \times magnification). (G) Quantitative assessment of caspase-3 and -7 cleavage following transfection of the same siRNA pools as above (measured by the CaspaseGlo kit, Promega). Red line indicates background levels of caspase cleavage in HFF-c-MYC cells. Results were normalized for cell number by the Alamar Blue assay.

which we designate MYC-synthetic lethal (MYC-SL) genes. To eliminate siRNAs that exhibited substantial growth inhibition properties in normal cells, siRNAs with $>50\%$ reduced viability in HFF-pBabe were eliminated from further consideration regardless of differential toxicity. This process left 102 MYC-SL gene hits for follow-up (Dataset S1).

Network analysis identified known connections [based on the Ingenuity-curated database between the hits (blue) and a pre-

assembled MYC core pathway (red)] (Fig. S1). About 50% of the MYC-SL hits had known connections with MYC and functionally related genes. For example, TRRAP is a direct MYC-binding partner that mediates recruitment of histone acetyltransferase to selective MYC-bound promoters (24). Several MYC-SL hits were linked to the basic transcriptional machinery (see TBP node in Fig. S1) including *POLR2E*, *POLR2I*, and *GTF2H4*. *CDK2* was also identified as a MYC-SL gene, a finding consistent with its

essential role in limiting MYC-induced senescence in a mouse model of tumorigenesis (25). Additionally, the identification of *PES1*, a gene involved in ribosomal biogenesis (26), among MYC-SL genes is consistent with the direct stimulation of rRNA synthesis by *c-MYC* (19) and with the “addiction” to elevated ribosomal function of MYC-induced lymphomas (27). The broad spectrum of potential MYC-SL genes thus reflects known MYC functions linked not only to chromatin modification such as *TRRAP*, *BRD4* (28), and *CECR2* (29), but also to metabolism (*ALDOA* and *PDK1*), DNA repair (*DDB2*, *GTF2H4*, *NEIL1*, *POLH*, and *RAD21*), apoptosis (*BNIP2*, *BOK*, and *MCL1*), and mitotic control (*WEE1* and *NEK2*) (Fig. S1 and Dataset S1).

For follow-up, we selected 49 MYC-SL genes on the basis of best-predicted druggability, potential involvement in cancer pathways, and ranking in differential toxicity. Highlighting the robustness of the screen, 48 of the 49 tested genes were confirmed with more than one siRNA and in an additional matched pair of HFFs (98% confirmation rate, see Dataset S2 for the list of validated and selected MYC-SL). p53 homolog 1 (*PES1*), cat eye syndrome chromosome region, candidate 2 (*CECR2*), and casein kinase 1 epsilon (*CSNK1e*), were further tested via lentiviral-mediated shRNA knockdown, which confirmed their differential growth inhibition in HFF-MYC versus HFF-pBabe control (Fig. 1 C and D). Examination of differential toxicity in HFF-MYC cells was carried out for the majority (41 of 48) of MYC-SL genes by assessing levels of DNA damage and apoptosis. siRNA-mediated knockdown of 12 (~25%) of the hits resulted in elevated γ -H2AX foci in HFF-MYC but not in control cells. This result indicates that induction of DNA damage is a significant consequence of the MYC-synthetic lethal interaction (Fig. 1E for quantitation and Fig. 1F for representative images; summarized in Dataset S2). This finding is consistent with the role of MYC in promoting genomic instability (30) and replication-associated damage resulting from an acceleration of S phase (20, 31). Additionally, siRNA-mediated knockdown of 34 of 41 MYC-SL genes induced caspase-3 and -7 cleavage in HFF-MYC but not in HFF-pBabe (Fig. 1G and Dataset S2). The fact that the results from the original high-throughput screen could be recapitulated using a combination of three knockdown protocols (siRNA pools, deconvoluted siRNA pools, and lentiviral shRNAs) as well as independent assays indicates the robustness of our screening platform.

Targeting Casein Kinase 1 Epsilon Leads to Tumor Regression in Preclinical Models of MYCN-Driven Neuroblastoma. To validate MYC-SL genes in a model of MYC-driven cancer, we selected

neuroblastoma cell lines with or without *MYCN* amplification. Amplification of *MYCN* in neuroblastoma is a clear driver of tumorigenesis and the strongest molecular marker of poor prognosis, used for treatment stratification (32, 33). The similar transcriptional programs and cellular phenotypes of both *c-MYC* and *MYCN* (34), and the finding that *MYCN* can replace *c-MYC* during murine development (35) supports the idea that synthetic lethal interactions could be conserved. We therefore screened neuroblastoma cell lines with (IMR-32) or without (SK-N-AS) *MYCN* amplification with siRNAs targeting the 48 confirmed MYC-SL genes. Twelve MYC-SL genes exhibited selective lethality in *MYCN*-amplified neuroblastomas (marked in blue in Dataset S2), indicating at least partial overlap of synthetic lethal interactions by both MYC family members in a cancer-cell setting. We chose to focus on one of these genes, *CSNK1e*, for preclinical validation according to several criteria. First, *CSNK1e* expression correlated with *MYCN* amplification in a set of clinically annotated neuroblastoma tumor samples (see Fig. 4B). Second, siRNAs or stable knockdown of *CSNK1e* ranked among the top genes for differential lethality in HFF-MYC versus HFF-pBabe, while exhibiting minimal toxicity to normal HFFs (~77%, Fig. 1D and Dataset S1), suggesting the possibility of a good therapeutic window. Third, pharmacologic inhibitors were readily available (36), enabling verification in preclinical models. The differential growth inhibition by *CSNK1e* knockdown in *MYCN*-amplified neuroblastoma cells was confirmed in vitro using conditional lentiviral vectors targeting *CSNK1e* with two different hairpins, in two *MYCN*-amplified cell lines (IMR-32 and SK-N-BE2) and a *MYCN*-nonamplified line (SK-N-AS) (Fig. 2A–C). The specificity of the lentiviral-expressed short hairpins was confirmed by measuring the relative levels of mRNA expression of the six known isoforms of *CSNK1* by qRT-PCR and by microarray analysis, both of which indicated that *CSNK1e* was the only gene whose expression was significantly reduced by the knockdown (Fig. S2 and Dataset S3).

As an in vivo preclinical validation model, SK-N-BE2 (*MYCN* amplified) neuroblastoma cells were transduced in vitro with either a control sh-expressing lentiviral vector or with sh*CSNK1e* 1 and injected into the flanks of immunodeficient mice. Once tumors became engrafted (8–10 mm, equal to ~300 mm³ volume), mice were exposed to doxycycline to induce RNAi, and tumor growth was measured over time. As shown in Fig. 2D, neuroblastoma growth was significantly impaired in three of four treated mice, validating in vivo the MYC-synthetic lethal relationship with *CSNK1e* through single gene knockdown. The short treatment window for mouse 3 was due to the presence of a large ulcerative tumor in the control

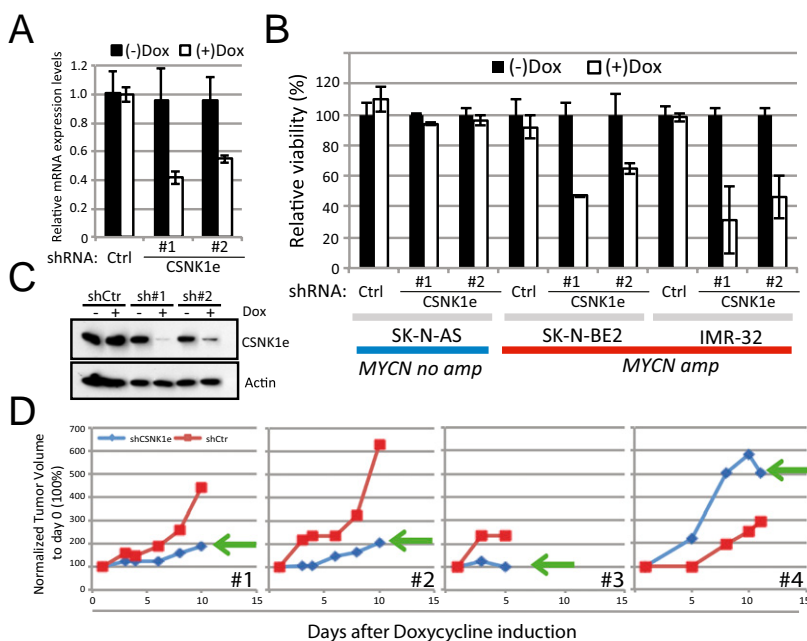


Fig. 2. *CSNK1e* knockdown impairs growth of *MYCN*-amplified neuroblastoma cell lines. (A) Relative levels of *CSNK1e* mRNA following doxycycline or DMSO treatment of neuroblastoma cell-line SK-N-BE2, harboring lentivirus expressing sh*CSNK1e* 1, 2, or sh control. Relative levels of each gene were calculated using the $\Delta\Delta$ CT method. *GAPDH* was used to normalize mRNA levels within each sample. (B) Viability assessment in two neuroblastoma lines, SK-N-BE2 and IMR32 (*MYCN* amplified) and SK-N-AS (*MYCN* not amplified) as measured by CellTiter Glo (Promega) following growth under DMSO or doxycycline-containing medium for 4 d. Values represent mean viability normalized to mock-treated cells. (C) Representative Western blot showing levels of *CSNK1e* protein in SK-N-BE2 cells shown in A. Actin is shown as a loading control. (D) Xenograft tumor growth of SK-N-BE2 cells transduced with doxycycline-inducible shRNA for *CSNK1e* or shControl in NOD/SCID mice. Doxycycline exposure was started when tumors reached a size of about 100 mm³. Knockdown of *CSNK1e* inhibited growth of established xenograft in three of four mice compared with no doxycycline-treated control (green arrows).

flank that forced the early termination of the drug treatment, whereas mouse 4 likely represented tumor cells escaping silencing.

We next proceeded to evaluate a small molecule inhibitor of CSNK1e enzymatic activity, IC261 (36). In vitro experiments had confirmed that MYC overexpressing cells were more sensitive to IC261 relative to cells with normal levels of MYC, with >100-fold differences in IC50 (Fig. S3 A, B, D, and E). IMR-32 (*MYCN* amplified) cells were used as a therapeutic xenograft model instead of SK-N-BE2, as the latter were established posttreatment and exhibit resistance to all chemotherapeutics (37). IMR-32 cells were highly sensitive to IC261 in vitro (Fig. S3B). A cohort of 10 xenograft-bearing mice was randomized into two groups with approximately equal tumor burden; one group was treated with daily s.c. injection of IC261 for 8 consecutive days, whereas the control group was treated with DMSO-vehicle only. IC261 was effective in halting tumor growth in all treated mice (Fig. 3B). A photograph of a representative mouse from each group before and after treatment is shown in Fig. 3A. Histopathological examination of the tumor tissue remaining after IC261 treatments, indicated a pronounced decrease in proliferation defect measured by BrdU labeling, whereas only modest apoptosis was detected via TUNEL assay at this time point (Fig. 3 C and D). However, the selective growth inhibition both in vitro and in vivo obtained by genetic knockdown and small-molecule inhibitor validate CSNK1e as a potential therapeutic target for *MYCN*-driven neuroblastoma. Recently, a more specific small-molecule inhibitor specific for CSNK1e as well as δ (delta) isoforms (PF-670462), became commercially available. *MYCN*-amplified and -nonamplified neuroblastoma cell lines were reassessed using this more specific inhibitor, and the results were consistent with that seen following treatment with IC261 (38) (Fig. S3C).

CSNK1e Expression Correlates with MYCN Amplification in Neuroblastoma and c-MYC in Adult Cancers. Through a metaanalysis of primary neuroblastoma microarray data, *CSNK1e* expression was found to correlate with both *MYCN* amplification and poor prognosis (<http://pub.abcc.ncicrf.gov/cgi-bin/JK>; Fig. 4 A and B). This correlation was confirmed in three representative cell lines at the protein level (Fig. 4C) and at the RNA level in these and additional cell lines (Fig. 4H). It is worth noting that neuroblastomas without *MYCN* amplification do indeed express *c-MYC*, which has been reported to be linked to WNT activity

(39) (Fig. 4 F and G). However, the levels of *c-MYC* are much lower than that present in HFF-MYC or *MYCN*-amplified neuroblastoma, as clearly indicated by qRT-PCR (Fig. 4G). The fact that CSNK1e knockdown did not affect the growth of *MYCN*-nonamplified neuroblastoma cell lines, is also consistent with the lack of up-regulation of CSNK1e in these cells. These results suggest that MYC-SL interactions here reported are selective for a high threshold of MYC overexpression (see Discussion).

Among the six *CSNK1* isoforms tested, epsilon up-regulation was present in all cells with *MYCN* amplification and it was also the predominant isoform expressed in these cells (Fig. 4H). These findings, as well as the presence of potential MYC-MAX binding sites in the promoter region of *CSNK1e* (Fig. S4), suggested that *CSNK1e* mRNA could be directly regulated by *c-MYC*/*MYCN*. Consistently, CSNK1e protein is up-regulated in both HFF-MYC (Fig. 4D) and upon induced *MYCN* expression in the neuroblastoma cell line Tet21N (40) (Fig. 4E). ChIP analysis of HFF-MYC cells indicated that *c-MYC* binds to at least two consensus sites, upstream and downstream from the transcriptional start site of the *CSNK1e* promoter, providing further evidence that the gene could be directly regulated by MYC (Fig. S4). However, we could not definitely demonstrate MYCN enrichment to the *CSNK1e* gene in neuroblastoma cells, possibly due to the high levels of MYCN protein not specifically bound to DNA. It is also likely that other factors contribute to the elevated transcription of *CSNK1e* in *MYCN*-amplified neuroblastoma. However, consistently with the hypothesis that *CSNK1e* expression is directly or indirectly linked to MYC overexpression, a metaanalysis indicated a significant positive correlation of both *c-MYC* levels and the *c-MYC*-associated "signature" with *CSNK1e* levels in colon, lung, and breast cancers (<http://www.intgen.org/expo/>; Fig. S5). Because CSNK1e exhibits synthetic lethality with MYC overexpression, its up-regulation particularly in MYC-overexpressing cancers, may be of functional significance.

Discussion

MYC-Synthetic Lethal Pathways. With the goal to identify therapeutic targets for MYC-driven cancers, this study reports the findings of a high-throughput arrayed siRNA screen from a collection of ~3,300 potentially druggable human genes as well as genes with cancer annotation. Prominent functional categories among the identified MYC-SL genes were related to DNA repair

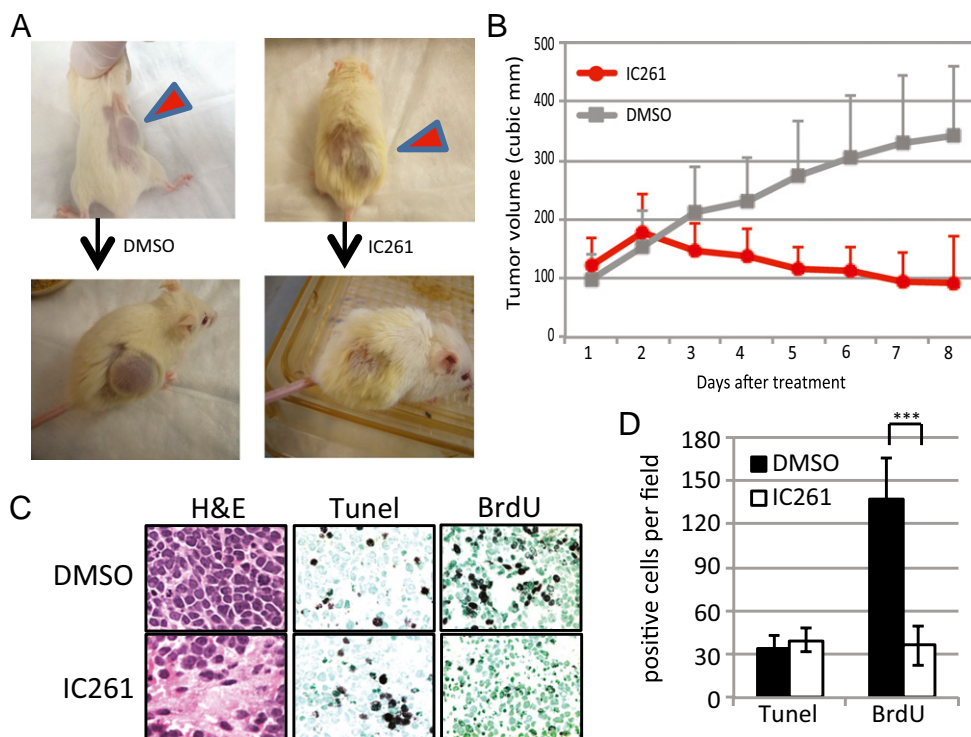


Fig. 3. IC261 treatment blocks *MYCN*-amplified neuroblastoma tumor growth in vivo. (A) Representative images of *MYCN*-amplified neuroblastoma xenograft obtained with IMR32 cells in NOD/SCID mice before and after treatment with either DMSO or IC261. Tumors were engrafted and allowed to reach a size of about 100 mm³, then IC261 (21.5 mg/kg) or DMSO was injected s.c. daily for 8 d. (B) Quantitation of tumor size over the 8-d treatment regimen with either IC261 or DMSO control. Values represent mean tumor volume at each time point ($n = 5$ for each group, error bars indicate SD). (C) Immunohistochemical analysis of tumor sections from IC261 and DMSO treatment groups described in A and B. Representative images of H&E, TUNEL, and BrdU staining for each group are shown. BrdU was administered 2 h before collection. (D) Quantitation of TUNEL⁺ and BrdU⁺ cells per field in DMSO- or IC261-treated xenograft tumors. Values represent mean number of positive cells per field, and error bars indicate SD of means.

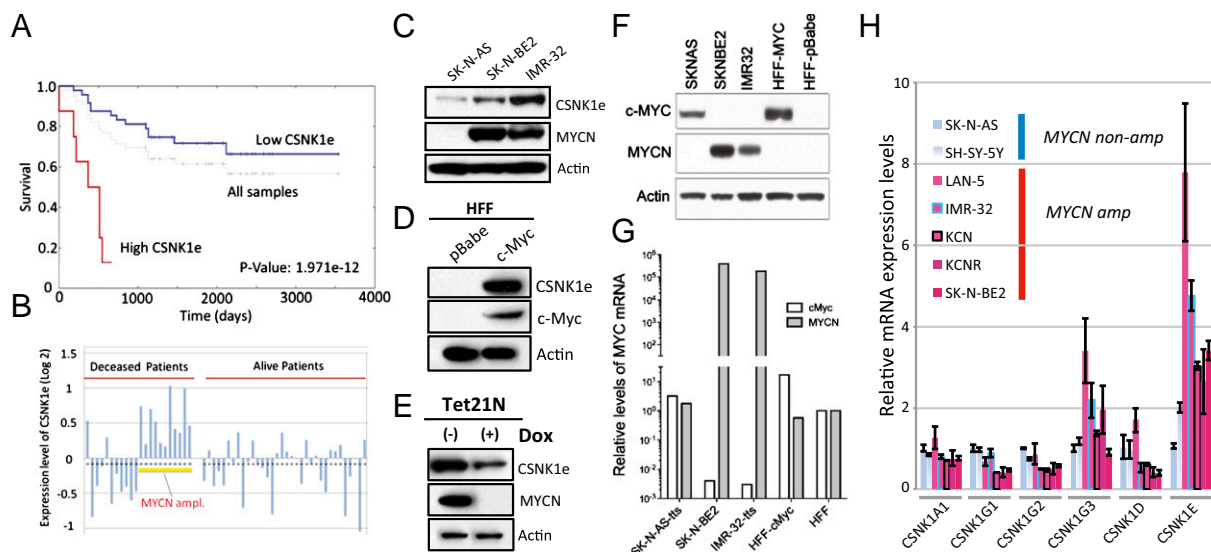


Fig. 4. CSNK1e expression correlates with poor prognosis and MYCN amplification in neuroblastoma. (A) Kaplan–Meier survival curves of neuroblastoma patients divided on the basis of CSNK1e expression; red indicates high expression and blue indicates low CSNK1e mRNA expression on the basis of microarray data accessible at the Oncogenomics neuroblastoma prognosis database (website: <http://pob.abcc.ncicrf.gov/cgi-bin/JK>). (B) Graphical representation of expression levels of CSNK1e mRNA, derived from the website above. Each bar represents expression level in one sample. Solid yellow line indicates samples derived from MYCN-amplified neuroblastoma. (C) Representative Western blot of CSNK1e, MYCN, and Actin (loading control) protein levels in SK-N-AS (MYCN not amplified), SK-N-BE2 and IMR-32 (MYCN amplified) neuroblastoma cells. (D) Representative Western blot of CSNK1e, MYCN, and actin (loading control) protein levels in HFF pBabe and HFF c-Myc cells. (E) Representative Western blot of CSNK1e, MYCN, and actin (loading control) protein levels in Tet21N (MYCN Tet-Off) cells in the presence or absence of doxycycline. (F) Representative Western blot of relative c-MYC and MYCN levels in SKNAS, SKNBE2, IMR-32, HFF-c-MYC, and HFF-pBabe. Actin is shown as a loading control. (G) Real-time RT-PCR quantification of c-MYC and MYCN mRNA levels from the cells in G. Values were calculated using the $\Delta\Delta\text{CT}$ method, and represent the mean fold change compared with HFF-pBabe, using GAPDH for normalization. (H) Real time RT-PCR quantification of the relative levels of each casein kinase I isoform in neuroblastoma cell lines with or without MYCN amplification. Relative levels of each gene were calculated using the $\Delta\Delta\text{CT}$ method. GAPDH was used to normalize mRNA levels within each sample.

(most enriched according to GeneGo), metabolism, apoptosis, basic transcription machinery, ribosomal RNA synthesis, mitotic control, and developmental pathways (Fig. S1 and Dataset S1). The screen also identified a known MYC interacting partner, TRRAP, involved in recruitment of histone acetyltransferase complexes to MYC-regulated target genes (41). In addition, two proteins involved in transcriptional elongation, such as the bromodomain protein BRD4 (28) and CDK12 (CRKS in Dataset S1) (42, 43), were among MYC-SL interactions. The recent utilization of bromodomain inhibitory molecules to target MYC-driven cancer models independently confirms the sensitivity of MYC-overexpressing cancer cells to BRD4 inhibition (44, 45). The role of complexes involved in transcriptional pausing/release among MYC-synthetic lethal is intriguing in light of recent demonstration of a role for c-MYC in this process in murine embryonic stem cells (46). Our findings suggest that a heightened dependence upon transcriptional elongation occurs only in the context of aberrant MYC expression, but not in normal cells. Finally, the enrichment in DNA-repair and -checkpoint genes (Dataset S1 for complete gene list) is consistent with the increased genomic instability and dramatic increase in the rate of DNA replication observed both in mammalian cells and in the *Xenopus* model system caused by MYC overexpression (20, 31, 47). MYC-SL genes related to DNA repair represent candidates for drug development with the potential to be used in combination with standard-of-care genotoxic treatments.

While this paper was under review, a study using the pooled lentiviral screening approach identified synthetic lethal interactions upon induction of a MYC-ER fusion in primary epithelial mammary cells (48). The results indicated a role in SUMOylation that influenced MYC transcriptional activity and exhibited synthetic lethality. Among the candidate genes reported by Kessler et al. (48) only one gene was in common with our screen result: BRD4; albeit others were in similar classes/function. Different cell systems (MYC-ER versus constitutive c-MYC), different screening methods (pooled shRNA versus arrayed siRNAs), and different libraries (sh against 30,000 genes versus siRNAs against 3,300 genes) could explain the lack of overlap. However, the high

reproducibility of the screen here reported (48 of 49 genes tested) underscores the accuracy of the one gene-per-well approach.

CSNK1e: A Druggable Gene Overexpressed in MYC-Driven Cancers.

We focused on CSNK1e as proof of principle to demonstrate the power to rapidly translate screening results to preclinical models. In fact, small-molecule inhibitors were readily available (36, 38), and CSNK1e expression significantly correlated with MYCN amplification in neuroblastoma. We also found that CSNK1e expression was associated with c-MYC in other tumor settings such as colon, lung, and breast cancer (Fig. S5). An independently derived link between MYC and CSNK1e was obtained through the genome-wide identification of modifiers of transcription factor activity through the MINDY algorithm, where CSNK1e scored as modifier of MYC target gene expression (49). CSNK1e was previously implicated in WNT and SHH (for review see ref. 50) and phosphorylation of PER to regulate circadian rhythms (51, 52), whereas only recently CSNK1e has been implicated in cancer (53–55). However, this is a unique demonstration of a functional link between CSNK1e and MYC to influence cancer growth and to implicate CSNK1e as a therapeutic target in MYC-driven cancers.

In the future, to stratify cancers that may benefit from CSNK1e inhibition other than MYCN-amplified neuroblastoma, it will be important to establish a threshold of MYC expression that could predict sensitivity to inhibition of CSNK1e. Perhaps the expression of CSNK1e itself could constitute a biomarker of sensitivity. Our study suggests that the ideal setting for therapeutics toward CSNK1e and perhaps other MYC-SL genes might be cancers where MYC expression is both intrinsically and prominently altered, such as consequent to gene amplification. In contrast, in instances where MYC expression is induced in the context of extracellular signaling pathways, those cancers may not be sensitive to inhibition of MYC-SL genes, but likely to respond to inhibition of MYC itself, as most proliferative cells. In summary, our study revealed candidates for therapeutic development identified through an efficient pipeline, which combined the power of high-throughput arrayed siRNA screening with optimized isogenic cell

pairs for target discovery, followed by validation in molecularly characterized cancer cells.

Materials and Methods

Cell Culture and Reagents. For the siRNA screen, primary human foreskin fibroblasts (HFF) transduced with pBabe-puro or pBabe-c-MYC-puro were utilized. Neuroblastoma cell lines were obtained from the American Type Culture Collection and from Dr. Susan Cohn (University of Chicago, Chicago, IL). The MYCN-inducible Tet21N cells were obtained from Robert N. Eisenman (Fred Hutchinson Cancer Research Center, Seattle, WA). For culture conditions and details see *SI Materials and Methods*.

siRNA Screen. For information regarding the siRNA library, transfection optimization, and read-out assay for high throughput screening see *SI Materials and Methods*.

DNA Damage and Apoptosis Assays. siRNA pools corresponding to the confirmed gene Hits were manually transfected in the HFF-pBabe-c-MYC and

HFF-pBabe-puro isogenic pair in 96-well format. Details for immunofluorescence detection of DNA damage and apoptosis can be found in *SI Materials and Methods*.

mRNA Expression by Real Time PCR, Western Blotting, Generation of shRNA Expressing Lentiviruses, Xenografts, and Immunohistochemical Staining. See *SI Materials and Methods*.

ACKNOWLEDGMENTS. We thank Dr. Susan Cohn for sharing her knowledge of the role of MYCN amplification in neuroblastoma and for cell lines; Kristin Robinson for maintaining cell cultures; Kay Gurley for histopathological analysis of tumors; Jody Carter, Bruce Clurman, Robert Eisenman, Hamid Bolouri, and Chris Kemp for critical reading of the manuscript; Travis Biechle and Daniel Diolaiti for discussions; and the Galloway laboratory for support and reagents. This work was supported by an award from the Ben Towne Endowment (to J.R.P.), R01 AG026661 from National Institute on Aging (to C.G.), and a Pilot Grant (to C.G.) from the National Cancer Institute Cancer Center Support Grant 5-P30 CA015704 to the Fred Hutchinson Cancer Research Center.

- Blancato J, Singh B, Liu A, Liao DJ, Dickson RB (2004) Correlation of amplification and overexpression of the c-myc oncogene in high-grade breast cancer: FISH, in situ hybridisation and immunohistochemical analyses. *Br J Cancer* 90:1612–1619.
- Sato H, Minei S, Hachiya T, Yoshida T, Takimoto Y (2006) Fluorescence in situ hybridization analysis of c-myc amplification in stage TNM prostate cancer in Japanese patients. *Int J Urol* 13:761–766.
- Kozma L, Kiss I, Szakáll S, Ember I (1994) Investigation of c-myc oncogene amplification in colorectal cancer. *Cancer Lett* 81:165–169.
- Park JR, Eggert A, Caron H (2008) Neuroblastoma: Biology, prognosis, and treatment. *Pediatr Clin North Am* 55:97–120, x.
- Chen CH, Shen J, Lee WJ, Chow SN (2005) Overexpression of cyclin D1 and c-Myc gene products in human primary epithelial ovarian cancer. *Int J Gynecol Cancer* 15:878–883.
- Takahashi Y, et al. (2007) Amplification of c-myc and cyclin D1 genes in primary and metastatic carcinomas of the liver. *Pathol Int* 57:437–442.
- Mitani S, et al. (2001) Analysis of c-myc DNA amplification in non-small cell lung carcinoma in comparison with small cell lung carcinoma using polymerase chain reaction. *Clin Exp Med* 1:105–111.
- Soucek L, et al. (2008) Modelling Myc inhibition as a cancer therapy. *Nature* 455:679–683.
- Hopkins AL, Groom CR (2002) The druggable genome. *Nat Rev Drug Discov* 1:727–730.
- Jiang H, et al. (2009) Stabilizers of the Max homodimer identified in virtual ligand screening inhibit Myc function. *Mol Pharmacol* 76:491–502.
- Trumpp A, et al. (2001) c-Myc regulates mammalian body size by controlling cell number but not cell size. *Nature* 414:768–773.
- Gomez-Roman N, Grandori C, Eisenman RN, White RJ (2003) Direct activation of RNA polymerase III transcription by c-Myc. *Nature* 421:290–294.
- Goga A, Yang D, Tward AD, Morgan DO, Bishop JM (2007) Inhibition of CDK1 as a potential therapy for tumors over-expressing MYC. *Nat Med* 13:820–827.
- Yang D, et al. (2010) Therapeutic potential of a synthetic lethal interaction between the MYC proto-oncogene and inhibition of aurora-B kinase. *Proc Natl Acad Sci USA* 107:13836–13841.
- Moser R, et al. (2012) MYC-driven tumorigenesis is inhibited by WRN syndrome gene deficiency. *Mol Cancer Res* 10:535–545.
- Kaelin WG, Jr. (2005) The concept of synthetic lethality in the context of anticancer therapy. *Nat Rev Cancer* 5:689–698.
- Benanti JA, et al. (2007) Epigenetic down-regulation of ARF expression is a selection step in immortalization of human fibroblasts by c-Myc. *Mol Cancer Res* 5:1181–1189.
- Benanti JA, Galloway DA (2004) Normal human fibroblasts are resistant to RAS-induced senescence. *Mol Cell Biol* 24:2842–2852.
- Grandori C, et al. (2005) c-Myc binds to human ribosomal DNA and stimulates transcription of rRNA genes by RNA polymerase I. *Nat Cell Biol* 7:311–318.
- Dominguez-Sola D, et al. (2007) Non-transcriptional control of DNA replication by c-Myc. *Nature* 448:445–451.
- Bartz SR, et al. (2006) Small interfering RNA screens reveal enhanced cisplatin cytotoxicity in tumor cells having both BRCA network and TP53 disruptions. *Mol Cell Biol* 26:9377–9386.
- Major MB, et al. (2008) New regulators of Wnt/beta-catenin signaling revealed by integrative molecular screening. *Sci Signal* 1:ra12.
- Chung N, et al. (2008) Median absolute deviation to improve hit selection for genome-scale RNAi screens. *J Biomol Screen* 13:149–158.
- Nikiforov MA, et al. (2002) TRRAP-dependent and TRRAP-independent transcriptional activation by Myc family oncoproteins. *Mol Cell Biol* 22:5054–5063.
- Campaner S, et al. (2010) Cdk2 suppresses cellular senescence induced by the c-myc oncogene. *Nat Cell Biol*, 12(1):54–59, sup pp 51–14.
- Lerch-Gaggl A, et al. (2002) Pescadillo is essential for nucleolar assembly, ribosome biogenesis, and mammalian cell proliferation. *J Biol Chem* 277:45347–45355.
- Barna M, et al. (2008) Suppression of Myc oncogenic activity by ribosomal protein haploinsufficiency. *Nature* 456:971–975.
- Jang MK, et al. (2005) The bromodomain protein Brd4 is a positive regulatory component of P-TEFb and stimulates RNA polymerase II-dependent transcription. *Mol Cell* 19:523–534.
- Banting GS, et al. (2005) CECR2, a protein involved in neurulation, forms a novel chromatin remodeling complex with SNF2L. *Hum Mol Genet* 14:513–524.
- Ray S, et al. (2006) MYC can induce DNA breaks in vivo and in vitro independent of reactive oxygen species. *Cancer Res* 66:6598–6605.
- Robinson K, Asawachaicharn N, Galloway DA, Grandori C (2009) c-Myc accelerates S-phase and requires WRN to avoid replication stress. *PLoS ONE* 4:e9591.
- Weiss WA, Aldape K, Mohapatra G, Feuerstein BG, Bishop JM (1997) Targeted expression of MYCN causes neuroblastoma in transgenic mice. *EMBO J* 16:2985–2995.
- Riley RD, et al. (2004) A systematic review of molecular and biological tumor markers in neuroblastoma. *Clin Cancer Res* 10:4–12.
- Boon K, et al. (2001) N-myc enhances the expression of a large set of genes functioning in ribosome biogenesis and protein synthesis. *EMBO J* 20:1383–1393.
- Malynn BA, et al. (2000) N-myc can functionally replace c-myc in murine development, cellular growth, and differentiation. *Genes Dev* 14:1390–1399.
- Mashhoon N, et al. (2000) Crystal structure of a conformation-selective casein kinase-1 inhibitor. *J Biol Chem* 275:20052–20060.
- Keshelava N, Seeger RC, Groshen S, Reynolds CP (1998) Drug resistance patterns of human neuroblastoma cell lines derived from patients at different phases of therapy. *Cancer Res* 58:5396–5405.
- Walton KM, et al. (2009) Selective inhibition of casein kinase 1 epsilon minimally alters circadian clock period. *J Pharmacol Exp Ther* 330:430–439.
- Liu X, et al. (2008) Deregulated Wnt/beta-catenin program in high-risk neuroblastomas without MYCN amplification. *Oncogene* 27:1478–1488.
- Lutz W, et al. (1996) Conditional expression of N-myc in human neuroblastoma cells increases expression of alpha-prothymosin and ornithine decarboxylase and accelerates progression into S-phase early after mitogenic stimulation of quiescent cells. *Oncogene* 13:803–812.
- McMahon SB, Wood MA, Cole MD (2000) The essential cofactor TRRAP recruits the histone acetyltransferase hGCN5 to c-Myc. *Mol Cell Biol* 20:556–562.
- Blazek D, et al. (2011) The Cyclin K/Cdk12 complex maintains genomic stability via regulation of expression of DNA damage response genes. *Genes Dev* 25:2158–2172.
- Bartkowiak B, et al. (2010) CDK12 is a transcription elongation-associated CTD kinase, the metazoan ortholog of yeast Ctk1. *Genes Dev* 24:2303–2316.
- Delmore JE, et al. (2011) BET bromodomain inhibition as a therapeutic strategy to target c-Myc. *Cell* 146:904–917.
- Zuber J, et al. (2011) RNAi screen identifies Brd4 as a therapeutic target in acute myeloid leukaemia. *Nature* 478:524–528.
- Rahl PB, et al. (2010) c-Myc regulates transcriptional pause release. *Cell* 141:432–445.
- Felsher DW, Bishop JM (1999) Transient excess of MYC activity can elicit genomic instability and tumorigenesis. *Proc Natl Acad Sci USA* 96:3940–3944.
- Kessler JD, et al. (2012) A SUMOylation-dependent transcriptional subprogram is required for Myc-driven tumorigenesis. *Science* 335:348–353.
- Wang K, et al. (2009) Genome-wide identification of post-translational modulators of transcription factor activity in human B cells. *Nat Biotechnol* 27:829–839.
- Price MA (2006) CKI, there's more than one: Casein kinase I family members in Wnt and Hedgehog signaling. *Genes Dev* 20:399–410.
- Badura L, et al. (2007) An inhibitor of casein kinase I epsilon induces phase delays in circadian rhythms under free-running and entrained conditions. *J Pharmacol Exp Ther* 322:730–738.
- Meng QJ, et al. (2008) Setting clock speed in mammals: The CK1 epsilon tau mutation in mice accelerates circadian pacemakers by selectively destabilizing PERIOD proteins. *Neuron* 58:78–88.
- Dolezal T, Kucerova K, Neuhold J, Bryant PJ (2010) Casein kinase I epsilon somatic mutations found in breast cancer cause overgrowth in *Drosophila*. *Int J Dev Biol* 54:1419–1424.
- Kim SY, et al. (2010) CK1epsilon is required for breast cancers dependent on beta-catenin activity. *PLoS ONE* 5:e8979.
- Yang WS, Stockwell BR (2008) Inhibition of casein kinase 1-epsilon induces cancer-cell-selective, PERIOD2-dependent growth arrest. *Genome Biol* 9:R92.

Supporting Information

Toyoshima et al. 10.1073/pnas.1121119109

SI Materials and Methods

Cell Culture and Reagents. The primary human foreskin fibroblasts (HFFs) and retroviral vectors (pBabe-puro and pBabe-c-MYC-puro) were as previously described (1). Cell were grown in DMEM (Gibco-BRI) with 1% (vol/vol) penicillin/streptomycin and 10% (vol/vol) FBS. Neuroblastoma cell lines: SK-N-AS, SK-N-BE2, and IMR-32 cells were obtained from American Type Culture Collection; SH-SY5Y, LAN-5, NBL-W-N, SMS-KCN, and SMS-KCNR were provided by Dr. Susan Cohn (University of Chicago, Chicago). MYCN-inducible Tet21N cells originally described by Lutz et al. (2), were obtained from Robert N. Eisenman [Fred Hutchinson Cancer Research Center (FHCRC), Seattle WA]. All neuroblastoma cells were grown in Roswell Park Memorial Institute (RPMI) 1680 medium (Gibco-BRI) with 25 mM of Hepes, L-glutamine, penicillin/streptomycin, and 10% (vol/vol) FBS. All cells were incubated humidified at 37 °C and 5% CO₂. All shRNA expressing stable cell lines were grown in the medium supplemented with 10% (vol/vol) Tet-approved FBS (Clontech). Doxycycline and IC261 were purchased from Sigma.

siRNA Screen. siRNA library. The siRNA library targeted ~3,311 unique human genes, with three siRNAs per gene and comprises a collection of druggable genes (3). It included the following classes of genes: kinases, phosphatases, ubiquitinating ligases, DNA repair proteins, as well as a set of custom-selected gene sets involved in cancer pathways (siRNAs were ordered from Sigma-Prologo). siRNA library sequences were designed with an algorithm developed to increase efficiency of the siRNAs for silencing while minimizing their off-target effects (4). Sigma-Aldrich has adopted this screening design algorithm and siRNAs targeting the druggable genome are now commercially available (MISSION prearrayed siRNA libraries).

siRNA transfection optimization. siRNAs transfection and readout timing were optimized to achieve a Z' factor for HFF-pBabe of 0.645 and for HFF-MYC of 0.726, using a negative control siRNA (siLuc) and a highly toxic siRNA, in this case targeting the kinesin motor protein Kif11. Briefly, the linear range for Alamar Blue assay for each cell type (HFF-pB and HFF-MYC) was defined by plating different cell concentrations. A matrix of 136 different conditions, including cell number, type of transfection reagent, siRNA ratio relative to transfection reagent, and final transfection amounts were also tested in duplicates. The readout timing was tested at 72 and 96 h. The conditions with best Z' factor were then used for screening as follow: Dharmafect 1 as transfection reagent at a ratio of 1:1 volume with siRNAs; the siRNA amount at 1.25 pmol, followed by a 96-h incubation. Plates were assayed for viability with Alamar Blue (~1.5–2 h incubation).

HTS screening conditions. HFF-MYC and HF-pB control cells were transfected with siRNAs using Dharmafect I with three siRNAs targeting the same gene pooled at equal molarity (final concentration of each siRNA, 17 nM; total siRNA concentration, 50 nM) to target one gene per well; the screen was carried out in triplicate replicas. Semiautomated transfections were carried out as described (5) with the following modifications: on day 1, cells were seeded in 384-well tissue culture plates (Matrix Technologies) at 400 (HFF-pB) and 200 (HFF-MYC) cells per well in 50 μ L per well of complete medium using a WellMate (Matrix Technologies); on day 2, cells were transfected using a Biomek FX and the plates were incubated at 37 °C in a 5% CO₂ incubator for 72 h; on day 5, (a total of 96 h from the time of plating) cell viability was determined using the Alamar Blue reagent (BioSource International) following the assay conditions previously described

(5). The plates were incubated for 1–4 h at 37 °C prior to measuring fluorescence (544-nm excitation, 590-nm emission) with an Envision multilabel plate reader (PerkinElmer). The fluorescence signal was corrected for background (no cells). Cell growth was expressed as percent viability relative to the median value of wells transfected with an siRNA to luciferase. Hits were determined by Z score ≥ 2 , calculated as described (6).

DNA Damage and Apoptosis Assays. siRNA pools corresponding to the confirmed gene hits were manually transfected in the HFF-MYC and HFF-pB isogenic pair in 96-well format using RNAi-Max (Invitrogen) transfection reagent in 100 μ L volume. The following day 100 mL of fresh media was added and plates were incubated for 48 h in a 37 °C 5% CO₂ incubator. Cells were then either fixed for immunofluorescence staining or assayed for apoptosis. For immunofluorescence detection of DNA damage, mouse anti-H2AX Millipore Anti Phospho-H2AX (Ser139, 07-164), was used as described with the modification that the fixation step was carried out while plates were centrifuged at 2,000 rpm for 30 min in a Sorvall Legend Centrifuge with a four place swinging rotor (Thermo Scientific 75006445) table-top centrifuge to minimize detachment during washing steps. Immunofluorescence signal within Hoechst-stained nuclei was quantitated using an INCell automated microscope, with a 10 \times objective, capturing five images per well. Nuclear fluorescence in control mock transfected samples was used to set a threshold for background fluorescence. Nuclei with fluorescence intensity above this negative threshold control was automatically counted in all fields. To measure induction of apoptosis following the siRNA transfection, Caspase-Glow 3/7 reagent was added to live cells (Promega) and luminescence was immediately quantified using the EnVision multilabel plate reader (PerkinElmer). Apoptotic readouts were corrected for cell density by normalization to parallel transfected plates where cells were quantified using with Alamar Blue staining.

mRNA Expression by Real-Time PCR. Total RNA was isolated using the RNeasy Mini kit (Qiagen) according to manufacturer's protocol, and the quantity and quality of the RNA was analyzed by the spectrophotometer. One microgram of total RNA was reverse transcribed using the SuperScript II (Invitrogen) and random hexamer primers (Invitrogen) at 42 °C for 50 min. Resultant cDNA was used in a quantitative real time-PCR with ABI 7900HT systems and pre-designed TaqMan probes (Applied Biosystems) for CSNK1e (Hs00266431_m1), PES1 (Hs00362795_g1), CECR2 (Hs00229989_m1), CSNK1a (Hs00793391_m1), CSNK1g1 (Hs00222804_m1), CSNK1g2 (Hs00176258_m1), CSNK1g3 (Hs00177858_m1), CSNK1d (Hs01020332_m1), and MYCN (Hs00232074_m1). Each determination of Ct values was done in triplicate and normalized with Ct value of triplicate measurements using TaqMan probes for GAPDH (ABI; 4352934) from the same samples. The comparative Ct method was used to determine gene expression levels.

Western Blotting. Preparation of whole cell lysates and Western blotting were performed as previously described (7) with the following antibodies: anti-CSNK1e (610445; BD Biosciences), anti-c-MYC (sc-42 and sc-764; Santa Cruz Biotechnology), anti-MYCN (NCM-II; Santa Cruz Biotechnology), antiactin (AC-15; Abcam). Quantitation of Western blot was performed using ImageJ software (National Institutes of Health).

Generation of shRNA Lentiviruses. Constitutive expressing short hairpin RNAs (shRNA) for CSNK1e, PES1, and CECR2 (1, 2,

and 3 for each gene), and nontargeting control (shControl) were cloned into the pLenti-viral vector pFUGW, as previously described (8). The core sequences of each shRNA are as follows:

CSNK1e no. 1 (GCAACCTGGTCTACATCATCG)
 CSNK1e no. 2 (GCTACGTGTCATGTACTTCA)
 CSNK1e no. 3 (GCCAGAAGTATGAACGGATCA)
 PES1 no.1 (GCCTTGAGAAGAAGAAGTATG)
 PES1 no. 2 (GCATTCTGAAGGGCATTATC)
 PES1 no. 3 (GCAAGGTCTTCTGTCCATCA)
 CECR2 no. 1 (GGAGTTAGAAGCCGCTCTTCA)
 CECR2 no. 2 (GCAGCTCCAGTTGGAATTAA)
 CECR2 no. 3 (GGAGAACAGTGAAGCACAAGA)
 shControl (CAACAAGATGAAGAGCACCAA)

To generate tet-inducible cell lines, neuroblastoma cell lines were first transduced with a lentivirus expressing tTS (tetracycline-controlled transcriptional repressor; Clontech) and selected with neomycin. The tTS-expressing cells were subsequently infected with an shRNA-expressing lentiviral vector derived from pLenti6 as described (9); shRNA and a scramble were designed and constructed in the pLenti6-tts system using the Gateway LR Clonase. The core target sequences used in doxycycline-inducible shRNA are as follows: CSNK1e sh no. 1 (GGCTATCCCTCCGAATTCT) and CSNK1e sh no. 2 (GAACGGATCAGCGAGAAGA). shRNA encoding plasmids were transfected into 293T cells with helper plasmids encoding gag-pol and vesicular stomatitis virus envelope glycoprotein using Fugene6 (Roche). Growth media was exchanged the following day and lentivirus containing supernatants were harvested and concentrated by centrifugation. Lentivirus stocks were tested on HT1080 fibrosarcoma cells and equivalent titers were used for infection of NB cells.

In Vivo Analysis. The NB cells, IMR-32 were counted, resuspended in 1:1 culture medium/Matrigel (BD Bioscience) on ice, and injected s.c. into the flank of 6- to 8-wk-old female NOD/SCID gamma null mice under protocol approved by the FHCRC committee (IRB no. 1712). After 4 wk, (tumor diameter of ~8–10 mm,

equal to ~300 mm³ volume) mice were randomized to the control group ($n = 5$) or the IC-261 treatment group ($n = 5$). Injection of dimethyl sulfoxide [10% (vol/vol) DMSO; control group] or IC-261 s.c. (20.5 mg/kg also in 10% DMSO) were performed daily for 8 d. For doxycycline-inducible knockdown experiments, SK-N-BE2 tTS cells infected with either the lentiviral tet-controlled shCSNK1e no. 1 or shControl were transduced in vitro. Two days following transduction, 2.5×10^6 cells in 0.2 mL PBS were inoculated s.c. into the left and right flanks of NOD/SCID gamma null mice ($n = 4$). After tumors were established, mice were exposed to doxycycline (2 mg/mL in 5% sucrose) ad libitum in their drinking water. The volume of the implanted tumor was measured every 2–3 d with a caliper, using the formula: $V = L \times W^2/2$, where V is volume (mm³), L is biggest diameter (mm), and W is smallest diameter (mm). Mice were killed by CO₂ inhalation the day after the last treatment and then tumors were fixed or frozen for further study.

Immunohistochemical Staining. Tissues were fixed in normal buffered formalin and subsequently processed to paraffin. Tissue sections of 4 μ m were deparaffinized, rehydrated, and stained for H&E, TUNEL, or BrdU. Sections for BrdU (Dako) staining were treated with HCl and trypsin before incubating with primary antibody. For TUNEL staining, TACS2 TdT kit (Trevigen) was used according to manufacturer's instructions. All bright-field images were captured using a Nikon Labophot-2 microscope with Spot Insight color camera and version 3.2 Spot Insight software (Diagnostic Instruments). All images shown are representative of at least 10 fields, viewed over two stained sections per animals. Quantitation was performed using 10 fields per animal.

Statistical Analysis. All columns represent mean \pm SDs, unless otherwise noted. All statistical analyses were performed using unpaired two-tailed t test unless otherwise indicated. Survival curves were constructed according to the Kaplan–Meier method and compared with the log-rank test. Graphpad Prism version 4.00 or SPSS (IBM) were used for statistical analysis.

- Benanti JA, et al. (2007) Epigenetic down-regulation of ARF expression is a selection step in immortalization of human fibroblasts by c-Myc. *Mol Cancer Res* 5:1181–1189.
- Lutz W, et al. (1996) Conditional expression of N-myc in human neuroblastoma cells increases expression of alpha-prothymosin and ornithine decarboxylase and accelerates progression into S-phase early after mitogenic stimulation of quiescent cells. *Oncogene* 13:803–812.
- Hopkins AL, Groom CR (2002) The druggable genome. *Nat Rev Drug Discov* 1:727–730.
- Jackson AL, et al. (2003) Expression profiling reveals off-target gene regulation by RNAi. *Nat Biotechnol* 21:635–637.
- Bartz SR, et al. (2006) Small interfering RNA screens reveal enhanced cisplatin cytotoxicity in tumor cells having both BRCA network and TP53 disruptions. *Mol Cell Biol* 26:9377–9386.
- Chung N, et al. (2008) Median absolute deviation to improve hit selection for genome-scale RNAi screens. *J Biomol Screen* 13:149–158.
- Robinson K, Asawachaicharn N, Galloway DA, Grandori C (2009) c-Myc accelerates S-phase and requires WRN to avoid replication stress. *PLoS ONE* 4:e5951.
- Xu M, Luo W, Elzi DJ, Grandori C, Galloway DA (2008) NFX1 interacts with mSin3A/histone deacetylase to repress hTERT transcription in keratinocytes. *Mol Cell Biol* 28:4819–4828.
- Chau BN, et al. (2009) Identification of SULF2 as a novel transcriptional target of p53 by use of integrated genomic analyses. *Cancer Res* 69:1368–1374.

Dataset S1. List of all gene hits here referred to as MYC-SL

[Dataset S1](#)

A total of 102 genes out of 148 hits remained after siRNAs with percent viability of <50% in control HFF-pB were eliminated. microRNAs are also not listed here. The indicated percent viability is the average of three replicates and is expressed as percent viability relative to the median value of wells transfected with an siRNA to luciferase. Hits were determined by Z score ≥ 2 , calculated as described in ref. 6. The last column refers to the ratio of percent viability of a given siRNA pool in HFF-pB/HFF-MYC.

Dataset S2. List of confirmed MYC-synthetic lethal genes

[Dataset S2](#)

Forty-nine genes among the 102 MYC-SL genes were selected because of druggability and best differential toxicity for further confirmation. Here shown are the 48 genes, which were confirmed by selective growth inhibition in an additional pair of matched HFF-c-MYC and control HFF-pB and with more than one siRNA upon deconvolution of the siRNA pool used in the screen. *CECR2 was confirmed by only one siRNA, but is listed here as it was confirmed by lentiviral-mediated silencing in HFF-MYC cells (Fig. 1).

Dataset S3. Microarray analysis following lentiviral-mediated knockdown of CSNK1e indicates that CSNK1e is the only significantly reduced gene

[Dataset S3](#)

MYCN-amplified SK-N-BE2 cells were transduced with lentiviral vectors expressing shCSNK1e no. 1 or shControl. Two days postinfection, cells were split and exposed to doxycycline to induce expression of the short hairpins and RNA was extracted at days 1, 2, and 3 from both shControl or shCSNK1e no. 1 and analyzed on the Illumina microarray platform. The ratio of gene expression for each gene after *CSNK1e* knockdown to control was calculated. As this was an exploratory experiment, a time course rather than three technical replicates was selected.